AJNR

Dynamic Susceptibility-Weighted Perfusion Imaging of High-Grade Gliomas: Characterization of Spatial Heterogeneity

Janine M. Lupo, Soonmee Cha, Susan M. Chang and Sarah J. Nelson

AJNR Am J Neuroradiol 2005, 26 (6) 1446-1454
http://www.ajnr.org/content/26/6/1446

AJNR Am J Neuroradiol 26:1446–1454, June/July 2005

Dynamic Susceptibility-Weighted Perfusion Imaging of High-Grade Gliomas: Characterization of Spatial Heterogeneity

Janine M. Lupo, Soonmee Cha, Susan M. Chang, and Sarah J. Nelson

BACKGROUND AND PURPOSE: **The advent of new anti-angiogenic therapies has created the need for better defining regions of abnormal vascularity in order to add specificity to the classification of high-grade gliomas. This study investigated MR imaging parameters corresponding to the peak height and percent recovery of the T2* relaxivity curve to characterize angiogenesis and microvascular leakage within the T2 and contrast-enhancing abnormalities in high-grade gliomas.**

METHODS: **Dynamic susceptibility-weighted MR imaging was performed in 41 patients with untreated high-grade glioma during the first pass and recirculation phase of a gadolinium bolus injection. Normalized peak height and percent recovery of the post-bolus signal were calculated on a voxel by voxel basis within the T2 and contrast-enhancing lesions (T2L, CEL) and compared between grade III and grade IV gliomas.**

RESULTS: **Grade IV gliomas showed significantly larger volumes of abnormal peak height and recovery compared to grade III patients ($P < .01$). Within the CEL, grade IV gliomas exhibited significantly higher peak height values than grade III patients ($P < .05$). Enhancing grade III patients (n = 7) demonstrated higher minimum values of percent recovery within both regions compared to grade IV patients. Non-enhancing grade III gliomas (n = 11) had significantly elevated minimum percent recovery values when compared to the T2L–CEL region in grade IV patients (n = 23; $P < .05$).**

CONCLUSION: **Direct measurement of the spatial distribution of tumor microvasculature characteristics has shown considerable heterogeneity within different regions of grade III and grade IV gliomas. Peak height and percent recovery parameters help to improve the specificity for characterization of the degree of angiogenesis and microvascular leakage in these tumors and may be useful in evaluating response to treatment.**

As gliomas grow and progress to a higher grade, the vascular supply is no longer adequate to support the increasing metabolic demands of the rapidly proliferating tumor cells (1). Regional hypoxia then ensues, leading to the upregulation of vasoactive endothelial growth factor (VEGF) and the promotion of new blood vessel formation from the existing vasculature, a phenomena known as angiogenesis (2–5). The new vessels that are formed often lack the complex structure of the normal brain vasculature and result in endothelial permeability. Tumor growth can also damage the existing vasculature and promote blood-brain-barrier breakdown (BBB) which results in microvascular leakage (6). Levels of VEGF and other angiogenic cytokines have been shown to escalate with increasing tumor grade (7, 8). This has led to the development of therapeutic agents designed to restrict tumor growth by inhibiting angiogenesis (9–12). With the advent of such anti-angiogenic therapies for the treatment of high grade gliomas, it is becoming increasingly important to be able to add specificity to the classification and localization of high grade gliomas based upon characteristics of their vasculature.

Quantification of parameters that can describe regions of angiogenesis and microvascular leakage noninvasively is thus considered a priority for planning and monitoring these therapies. The most widespread method for assessing leakage of the blood-brain bar-

Received August 12, 2004; accepted after revision December 22.

From the Departments of Radiology (J.M.L., S.C., S.J.N.) and Neurological Surgery (S.C., S.M.C.), University of California, San Francisco.

Supported by grants P50 CA97297 (SPORE: National Cancer Institute) and LSIT-01–10107 (US Discovery Grants, UC Office of the President, Berkeley, CA).

Presented at the International Society for Magnetic Resonance in Medicine, Kyoto, Japan, May 15–21, 2004.

Address reprint requests to Janine M. Lupo, UCSF Radiology, QB3 Building, 1700 4th Street, San Francisco, CA.

rier has been the presence of increased signal intensity on T1-weighted images after an injection of a gadolinium-based contrast agent. Although the presence of contrast enhancement on these images indicates regions where the BBB has been compromised by the tumor, it may also reflect areas of inflammation, necrosis, or response to radiation treatment (13, 14). Alternative approaches have been to make measurements of hemodynamic brain characteristics such as relative cerebral blood volume (rCBV). These studies, in combination with the evaluation of microvascular density (MVD) from histological sections, have been able to show that blood vessel density increases with tumor grade (15–17).

Dynamic susceptibility-weighted perfusion MRI is one technique that is commonly used to estimate rCBV through examination of the degradation of signal intensity over time associated with a bolus of a paramagnetic contrast agent such as gadolinium DTPA (12, 16, 18–24). During the first pass of this bolus, the signal intensity drops on T2*-weighted images and then recovers as the agent recirculates. The T2* signal intensity time series is converted to the change in relaxation rate or T2* relaxivity ($\Delta R2^*$), which is proportional to concentration at the doses typically used for patient studies (14, 16, 19–21, 23, 25–29). Traditional calculations from the dynamic data attempt to estimate the elevated blood volume in a given region relative to normal white matter (rCBV) by taking the area under the concentration vs. time curve (30). The estimation of rCBV using this method relies on the assumption of an intact blood-brain-barrier (BBB), which is typically not true for most high grade gliomas.

Numerous studies have attempted to correct for the under or over estimation of rCBV measurements from dynamic susceptibility-weighted perfusion MRI in regions of microvascular leakage and to derive new parameters to more accurately characterize endothelial permeability (14, 19, 21, 22, 24, 27–29). These include methods that can distinguish the boundary between the first pass bolus and recirculation, such as baseline subtraction (19) or using a non-linear algorithm to fit a gamma variate function, to help eliminate the effects of leakage into the extravascular space (19–21). These non-linear fitting procedures are typically unstable in portions of the image with low signal to noise ratio. More robust attempts to separate rCBV and relative permeability involve generating a model function of the signal as a sum of two components corresponding to the opposing T1 and T2* effects and then implementing a linear fitting method to estimate the properties of each component (14, 22, 24, 31). Other approaches have examined changes in the recirculation phase of bolus tracking using a relative recirculation (rR) parameter as a measure of vascular tortuosity and leakage. Estimates of rR correlate with tumor grade and have been utilized in assessing response to therapy (23, 27–29).

T1-weighted dynamic contrast enhanced MRI with pharmacokinetic modeling can be implemented to measure the concentration of contrast medium within the plasma and the rate at which the volume transfers to the extravascular-extracellular space, known as K^{trans} (32–36). However, this model requires multiple assumptions to accurately characterize the underlying physiology, and much longer imaging times are required in order to reach steady-state equilibrium, often making it difficult to separate intra and extra vascular components (34). Although T1 methods can achieve estimates of vessel wall permeability, T1 weighted acquisitions cannot be implemented on a fast enough time scale to directly measure the first passage of a contrast agent bolus, and the compartmental modeling used requires several assumptions and extrapolation to infer blood volume measurements. Dual echo techniques allow for quantification of various parameters by accounting for T1 effects of the contrast agent in the interstitial tissue (37–40), but have limited coverage, and hence prevent the characterization of spatial variations in the microvasculature of heterogeneous tumors. A T2* gradient echo, echo planar imaging technique was favored in this study because we are interested in capturing the first pass bolus behavior and comparing changes that occurred before, during, and immediately after injection of a paramagnetic contrast agent. This method can also be easily implemented in routine clinical practice where both short scan times and robust results with minimum computation are important factors in order for the data to be immediately incorporated into patient management.

Various groups have compared rCBV and/or permeability in low and high grade brain tumors. In the majority of these studies, the values used in the analysis have been obtained by a radiologist manually defining three or four ROI's ($\sim$60 mm^3) in the center of the tumor from the post-contrast T1-weighted imaging and then finding the region with the maximum rCBV or permeability compared to the contralateral white matter (16, 17, 19–21, 31, 41, 42). It has also been shown previously that the point of maximum signal drop (MSD) on the T2* signal time curve both is correlated with rCBV values and is a more stable measure of vessel volume in brain tumors (26). The purpose of our study was to investigate values obtained on a voxel by voxel basis using a non-parametric model corresponding to the peak height and percent recovery of the T2* relaxivity curve, in order to characterize heterogeneity in patterns of angiogenesis and microvascular leakage in regions of T2 abnormality and contrast enhancement for patients with grade III and grade IV gliomas.

Methods

Patients

MR imaging was performed on 41 untreated brain tumor patients (20 female, 21 male) immediately prior to surgery. Histopathologic analysis of the resected tissue confirmed the diagnosis of 18 grade III gliomas (median age 47) and 23 grade IV gliomas (median age 54). All patients provided informed consent using a protocol approved by our Institutional Review Board.

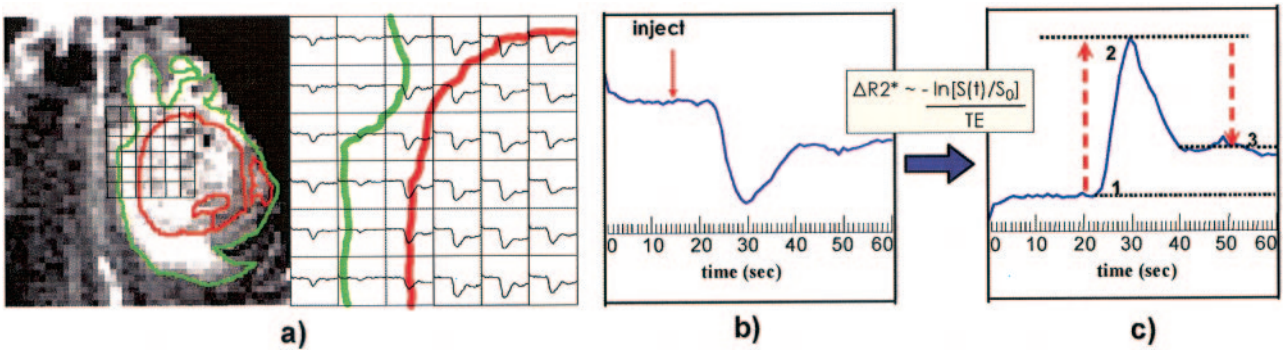

FIG 1. *A*, T2 and contrast enhancing contours overlaid on a GRE EPI and corresponding resampled T2* signal intensity time curves. *B*, Plot of T2* signal intensity time curve, S(t), for one voxel with red solid arrow denoting the time of contrast agent injection. *C*, Relative concentration curve obtained. Peak height is the distance from 1 to 2, while percent recovery represents how much the post-bolus signal (3) has recovered from the peak (2).

Magnetic Resonance Imaging

MRI exams were performed on a 1.5 T Signa Echospeed scanner (GE Medical Systems, Milwaukee, WI). The MR imaging protocol consisted of a three-plane localizer (8.5/1.6 ms [TR/TE]), axial fluid-attenuated inversion recovery (FLAIR; 10,000/148/2200 ms [TR/TE/TI]), axial 3D fast spin-echo T2-weighted imaging (FSE; 3000/102 ms), dynamic susceptibility-weighted, gradient-echo, echo planar imaging (EPI; 1000-1250/54 ms, flip angle 35°), and post-contrast 3D spoiled gradient-recalled (SPGR; 34/8 ms) T1-weighted imaging. The T2-FLAIR, FSE, and post contrast T1-SPGR images were acquired and used to define regions of T2 hyperintensity and T1 enhancement.

For the dynamic EPI series, the location and size of the tumor and the position of the superior and inferior margins were determined from the T2-weighted FLAIR or FSE images. Seven or eight slices were selected to cover the majority of the tumor volume. Slice thickness ranged from 3 to 5 mm and slice gap 0 to 2 mm. A standard dose of 0.1 mmol/kg body weight of gadopentetate dimeglumine (Gd DTPA) was injected intravenously with an MR-compatible power injector at a rate of 5 ml/s, followed immediately by a 20-ml continuous saline flush. A series of T2*-weighted multi-slice image sets (with a 26 × 26 cm^2 in plane FOV and 128 × 128 acquisition matrix) were acquired every 1–1.25 seconds during the first pass of the contrast agent until 60 time points were obtained.

Image Processing

The FLAIR/FSE, post-contrast 3D SPGR, and raw T2*-weighted echo planar images were transferred to a UNIX workstation (Sun Microsystems, Mountain View, CA) for off-line post-processing. Image processing was performed by using in-house software written in C and IDL programming languages (Research Systems, Inc., Boulder, CO). The FLAIR/FSE and post-contrast 3D SPGR images were resampled to the same slice locations and resolution as the echo planar perfusion images. The dynamic dataset was aligned to the anatomical images using affine and perspective transformations and, where necessary, non-rigid B-spline warping (43) by maximization of normalized mutual information (44). The co-registered perfusion series was then resampled to a 32 × 32 grid in-plane with a 16 x 16 cm^2 FOV so that the observed signal changes had sufficient signal to noise ratio to be analyzed reliably on a voxel by voxel basis. The pixel size was increased to a 5 × 5 mm^2 resolution in order to ensure that errors in the alignment to anatomical images due to geometric distortion would be contained within one voxel. This oversampling was comparable to most other studies that draw several ROIs (12, 19, 21, 31, 41, 42), each encompassing approximately twenty 2 × 2 mm^2 voxels, in order to obtain several rCBV or permeability measurements in the same region from which to calculate a maximum value.

For each tumor, ROIs were drawn around the contrast enhancing and T2 lesions from the resampled post-contrast injection 3D SPGR and either FLAIR or FSE images, respectively. Regions of signal dropout due to susceptibility on the echo planar images were excluded from the ROIs. All ROIs were approved by an attending neuroradiologist certified by the American Board of Radiology with a Certificate Added Qualification in neuroradiology (S.C.). The resampled echo planar image for a single slice of the first image set and corresponding T2* signal intensity time curves is displayed in Figure 1a, with overlaying contours depicting the extents of the T2 lesion, T2L (in green), and contrast enhancing lesion, CEL (in red).

Analysis of T2 Signal Intensity Time Curves*

The T2* signal time curve acquired during the first pass of gadolinium bolus was converted to the change in relaxation rate (ΔR2*). The pre-contrast baseline signal, S_0, was established from six image volumes acquired prior to contrast injection. Since the relative Gd-DTPA concentration is proportional to the ΔR2* curve, a plot of the relative concentration of Gd-DTPA in tissue over time was obtained for each voxel as exhibited in Figures 1b-c.

Subsequent analysis of the ΔR2* curves was performed utilizing in-house programs created with Matlab 6.5 software (MathWorks Inc., Natick, MA) as shown by Figures 1c and 2a-c. In order to normalize intensity differences between scans, the ΔR2* curve was divided by the intensity value at the second peak of the image histogram obtained from the first time point of the echo planar image series. Peak height and percent recovery of the post bolus signal from the maximum ΔR2* signal were determined for each voxel within the T2 and contrast enhancing (CE) lesions. Percent recovery was calculated as the difference between the peak height and average post-bolus signal divided by the peak height signal on the ΔR2* curve.

A model curve function was derived from averaging the time series data derived from normal appearing brain using the following automated approach. Voxels from the first pre-contrast echo planar image volume were arranged in a histogram based on their image intensity. A varying range of intensities, based on the maximum intensity and histogram peak was experimentally established to select the image intensities that corresponded only to normal brain tissue. This method proved to be robust and was able to successfully exclude curves within the T2 and contrast enhancing lesions, as well as ventricles, large veins, and necrotic regions. The reliability of the model function generation was assessed in several patients by comparing it to the averaged ΔR2* curves within manually-drawn

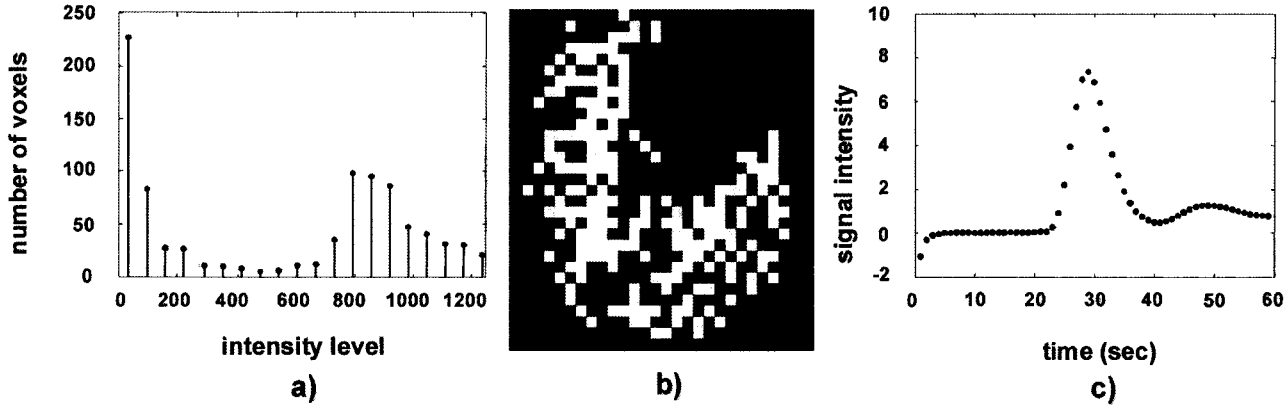

FIG 2. *A*, Histogram of intensities for the first time point, used to exclude tumor, ventricles, and large vessels from normal appearing brain tissue. *B*, Normal voxels selected using histogram analysis. *C*, The model function that results from averaging ΔR2* curves for all voxels displayed in *B*, used to normalize peak height values between patients.

white matter ROIs. In all of the patients examined, the automated model function was within the range of curves generated from both the whole brain and white matter ROIs.

The model curve function was used to normalize and threshold peak height and percent recovery maps. Voxels with peak height values greater than twice the model curve were classified as having abnormal peak height (aPH), while those whose post-bolus concentration recovered less than 75% from the peak concentration were considered to have abnormal recovery (aRec). Regions with no signal drop (NSD), as characterized by a flat signal on the time series data, were excluded from the calculations in order to avoid spurious results. NSD voxels were defined as having both low peak height (<.05) and poor correlation ($r < .25$) with the model function.

Volumes of aPH, aRec, NSD, and contrast enhancement were calculated and normalized according to the T2 lesion volume within the perfusion images. Mean and maximum peak height values, as well as mean and minimum percent recovery (the lowest percent recovery value within a given region, indicating the greatest amount of BBB breakdown), were calculated within the contrast enhancing lesion (CEL), T2 lesion (T2L), and T2 lesion excluding contrast enhancement (T2L –CEL) for each patient individually and then averaged across patients within each cohort. Voxels from all patients of the same grade were then combined for each region and mean values of parameters were computed. Statistical significance of group comparisons was determined through the use of a Wilcoxon ranked sum test. P-values less than .05 were considered significant. Data were expressed as the mean ± the standard deviation.

Results

All patients had large regions of T2 hyperintensity that were assumed to correspond to the area at risk for increased angiogenesis. Seven of the eighteen patients with grade III lesions and all twenty-three patients with grade IV lesions exhibited enhancement on the T1-weighted post-contrast SPGR image. While the intention was to cover the entire region of T2 hyperintensity for each lesion, the limited number of slices that could be acquired for the dynamic imaging meant that this was not always possible. The spatial extent of regions with abnormal MR parameters was therefore expressed as a percentage of the portion of the T2 lesion that was covered. The percentages of this region that were enhancing on the T1-weighted post-contrast images were significantly greater for the patients with grade IV gliomas than for patients with enhancing grade III lesions. Twenty-one of the twenty-three patients with grade IV lesions also had central regions of hypointensity on the post gadolinium T1-weighted images that were interpreted as suggesting necrosis. Similarly, grade IV gliomas also showed a significantly larger volume of NSD compared to grade III patients (Table 1).

TABLE 1: Volumes of abnormality expressed as percentages of the lesion on T2-weighted imaging

Finding	Grade III	Grade IV	*P* Value
Contrast enhancing	9.8 ± 12.3	32.7 ± 18.5	<.01
No decrease in signal intensity	7.6 ± 10.7	21.6 ± 22.7	<.02
Abnormal peak height	13.0 ± 10.0	24.9 ± 15.8	<.01
Abnormal recovery	10.1 ± 16.7	22.7 ± 16.9	<.001

Volumes with abnormal peak height and recovery

There was considerable heterogeneity in the dynamic concentration curves and the abnormal recovery within a grade III and grade IV glioma as showed in Figure 3. The volumes of aPH and aRec were significantly greater for grade IV than grade III gliomas (Table 1).

Peak Height

Within the CEL, grade IV gliomas exhibited significantly higher mean and maximum relative peak height values than enhancing grade III patients (Table 2). This was mainly due to the significantly elevated maximum peak height values (5.7, $P < .01$) outside the CEL for the grade III cohort. Mean peak height values, however, were similar for both regions of grade III tumors (1.2 for the CEL and 1.1 for the T2L–CEL). Grade IV patients exhibited elevated mean peak height values within the CEL compared to the T2L–CEL (2.0 vs. 1.2, $P < .001$), but the maximum peak height values were comparable (6.0 vs. 5.8). There was no significant difference in mean or maximum peak height values between grade III and grade IV populations in the T2L–CEL region. Anal-

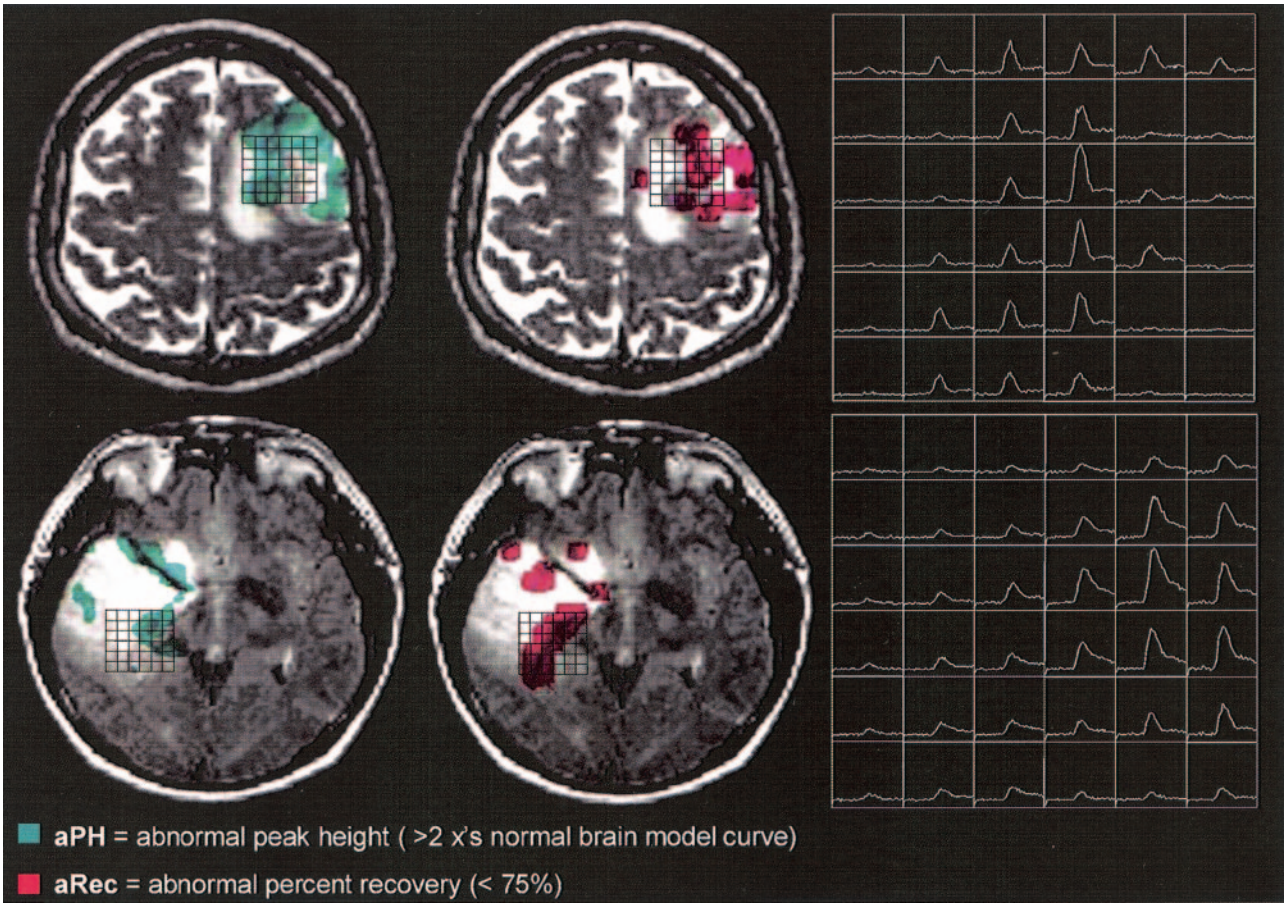

FIG 3. Example of abnormal peak height (aPH; *left*) and abnormal recovery (aRec; *center*) maps for grade IV (*top*) and grade III (*bottom*) gliomas overlaid on a T2-weighted image (*top* – FSE, *bottom* – FLAIR) and the ΔR2* curves from which they were derived (*right*). The grade IV glioma demonstrates a large area of aPH (green) and aRec (magenta) near the center of the lesion while in the grade III glioma both aPH and aRec are more peripherally located.

TABLE 2: Relative peak height and recovery values in and surrounding contrast-enhancing lesions

Finding	Grade III	Grade IV	*P* Value
Relative peak height			
Contrast enhancing			
Mean	1.2 ± 0.8	2.0 ± 0.9	<.5
Maximum	2.3 ± 1.6	6.0 ± 3.2	<.002
T2 − enhancing			
Mean	1.1 ± 0.4	1.2 ± 0.5	>.99
Maximum	5.7 ± 2.7	5.8 ± 2.6	>.5
Percent Recovery			
Contrast enhancing			
Mean	80.4 ± 11.4	77.5 ± 6.7	<.01
Minimum	71.1 ± 13.4	47.7 ± 17.6	>.1
T2 − enhancing*			
Mean	83.7 ± 6.2	82.2 ± 4.7	>.1
Minimum	56.1 ± 14.6	43.3 ± 18.5	>.5

TABLE 3: Relative peak height and recovery values for all voxels

Finding	Grade III	Grade IV	*P* Value
Relative peak height			
Contrast enhancing	1.1 ± 0.9	2.1 ± 1.6	<.001
T2 − enhancing	1.0 ± 0.9	1.2 ± 1.0	>.1
Percent Recovery			
Contrast enhancing	82.5 ± 10.5	76.4 ± 11.8	<.001
T2 − enhancing*	84.9 ± 8.8	80.9 ± 10.6	<.01

TABLE 4: Relative peak height and recovery values for nonenhancing lesions on T2-weighted images

Finding	Nonenhancing, Grade III	T2 − Enhancing,* Grade IV
Relative peak height		
Mean	1.2 ± 0.4	1.2 ± 0.5
Maximum	5.7 ± 2.8	5.8 ± 2.6
Recovery (%)		
Mean	86.4 ± 3.4	82.2 ± 4.9
Minimum	58.8 ± 12	43.3 ± 18.5

* T2 lesion excluding contrast enhancement.

ysis of voxels from all patients combined in a given region did show a significant increase in mean peak height in the T2L-CEL region for grade IV patients (see Table 3). Although the maximum peak height value lay outside the region of enhancement for all enhancing grade III patients, 61% of grade IV patients showed maximum peak height within the CEL. Table 4 shows that there was no significant difference in relative peak height values between the T2L of non-enhancing grade III gliomas and the T2L surrounding the CEL in grade IV tumors.

Percent Recovery

As expected, there was no significant difference in the recovery of the model function between grades ($P > .8$), with grade III = 82.5 ± 4.9% and grade IV = 83.1 ± 4.0%, since it is derived by averaging normal voxels. Decreasing trends were observed with higher grade for both the minimum and mean percent recovery values in all regions (Table 2). However, this reduction was only significant ($P < .01$) for minimum recovery values within the CEL. Within the grade III cohort there was a significantly lower minimum recovery of 56.1% in the T2L surrounding the area of enhancement ($P < .03$), compared to 71.1% recovery within the CEL. When comparing all voxels in a specified region grouped together across patients, all of the observed trends for mean recovery values become significant, with voxels of grade IV gliomas having a lower mean recovery than grade III voxels and CEL voxels having a lower mean percent recovery than T2L–CEL voxels for each grade (Table 3). The minimum recovery value was outside the CEL for all enhancing grade III patients, but minimum recovery was within the CEL for 22% of the patients with grade IV lesions. Patients with non-enhancing grade III gliomas had significantly higher minimum recovery than the T2L –CEL region in grade IV patients (58.8% vs. 43.3% with $P < .03$, Table 4).

Discussion

The degree of angiogenesis and microvascular leakage are important physiological parameters that can provide insight to the malignant potential of tumors. Dynamic susceptibility-weighted perfusion MRI is able to provide maps of peak height and percent recovery that contain information about these physiological processes. A noteworthy feature of this approach is that it is a fast method in which the calculations do not rely on any prior assumptions as to the biology of the model that they describe. By investigating the two parameters peak height and percent recovery independently, confounding corrections of rCBV and K^{trans}, as well as other permeability measures, can be removed while separating first-pass bolus characteristics from the recirculation phase. Our analysis of data from patients with grade III and grade IV gliomas has shown that there is spatial heterogeneity in these parameters for both the region of contrast enhancement (CEL) and the surrounding region of hyperintensity on T2-weighted images (T2L-CEL). Our goal was to gain insight as to how different regions of each tumor type behave, in addition to differentiating between the two astrocytic tumor grades. While the presence of such heterogeneity is not surprising based upon the known histological characteristics of these tumors, the fact that it can be measured non-invasively is novel and likely to be important for the clinical management of individual patients. Identifying certain regions of a grade III tumor that have similar vascular features to a grade IV tumor would be useful in determining the more aggressive part of the tumor for planning therapy. This heterogeneity, however, also underlines the potential limitations in describing the characteristics of the tumor from measurements made by considering small regions of interest or by averaging values across the entire T2L.

The choice of metrics to describe the shape of the dynamic data was dictated by our desire to minimize the dependence on complex, non-linear fitting procedures and to provide robust estimates of meaningful parameters. The calculations of peak height and percentage recovery are simple to implement and are relatively insensitive to signal to noise ratio. Although there was some variation in observed peak widths, the time to peak was remarkably similar (within one time point) for both the normal and tumor voxels. This suggested that there was a close correspondence between the peak heights and the underlying rCBV. The observation of abnormal recovery in the T2L-CEL suggests that this parameter may be more sensitive to the presence of abnormal vasculature than conventional post-contrast images. Whether this is due to increased vessel tortuosity or to a more reliable measure of vascular permeability is yet to be determined.

The measurement of rCBV in tumors is complicated in regions where the blood-brain-barrier is compromised. The leakage of contrast agent into the extra-vascular space leads to additional changes in signal intensity on the echo planar images. The first effect is an increase in intensity based upon the reduction in T1 of the tissue and the second effect is a decrease in intensity due to increased susceptibility-induced T2* shortening. We chose gradient echo, EPI with a low flip angle (35°), so that the susceptibility-induced T2* shortening of the leaking contrast agent predominates, preventing an overshoot of the baseline signal. As a result, the recovery of the model function for normal tissue ranged from 77% to 90% across all patients (with the exception of one outlier), regardless of tumor grade, and recovery values of less than 75% were considered abnormal. A cutoff of twice the model peak height was selected to define what was considered abnormal peak height or vessel volume, since it has been shown that the blood volume of gray matter, and subsequently the peak height of the $\Delta R2^*$ curve, is two to three times that of white matter (19, 26). The peak height of the model function would therefore be approximately 1.5 times that of normal white matter tissue, since the model function is derived from voxels comprising both white matter and the portion of gray matter excluding large vessels. Thus, a threshold of twice the model function height should be a reliable indicator of abnormal blood volume.

The volume of contrast enhancement on post-gadolinium T1-weighted images has been previously shown to increase with tumor grade (13), as our results also confirm. Besides signifying a disruption of vascular integrity, the presence of contrast enhancement can indicate either active tumor or macroscopic necrosis. The observed increase in NSD volume with glioma grade was expected since regions of NSD are devoid of vasculature and are likely to coincide with

necrotic regions, the presence of which is indicative of grade IV tumor. The significantly larger volumes of aPH and aRec for grade IV gliomas support the idea that there is a global increase in angiogenesis and BBB breakdown in the microvasculature of grade IV gliomas.

Both grade III and grade IV patients exhibited abnormal vessel volume outside the CEL, as indicated by elevated peak height values (Tables 2 and 3). That the maximum peak height values were lower within the CEL for enhancing grade III gliomas, suggests that there is increased angiogenesis in portions of tumor outside the CEL. This interpretation is consistent with elevated blood volume preceding the appearance of enhancement (45). In grade IV patients, it appears that increased vessel volume is more likely to be localized to the enhancing region based on the mean peak height values. The presence of contrast enhancement in grade IV patients represents a combination of tumor plus necrotic tissue, rather than reflecting BBB breakdown due to tumor alone. The elevated mean peak height values exhibited by grade IV patients and the fact that this increase was localized to the enhancing region can be attributed to the local hypoxia and is a known promoter of angiogenesis (2–5, 8, 46). The two patient populations had similar peak height values within the edema that surrounds the enhancing tumor. Comparison of voxels across all patients did reveal a significant difference in mean peak height (.1), even though relative peak height values between the T2L of non-enhancing grade III gliomas and the T2L surrounding the CEL in grade IV tumors were similar, as shown in Table 4. Although there have been several studies suggesting an increase in angiogenesis outside the CEL in grade IV gliomas compared to metastatic brain tumors (47, 48), to our knowledge there has not been any published results that radiographically investigate angiogenesis in non-enhancing regions of grade III gliomas with respect to the enhancing region of the same tumor and the similar-appearing non-enhancing portion of grade IV gliomas. The fact that we found comparable elevated peak heights in the surrounding T2 lesion of grade III gliomas as in the same region in grade IV gliomas even though these same grade III patients exhibit significantly reduced peak height within the CEL, is therefore both novel and significant.

As expected, we observed reduced mean percent recovery values in regions of contrast enhancing tumor for both patient populations. The lower mean percent recovery values observed in patients with grade IV gliomas was consistent with the elevated CEL volume observed in these patients (Table 1). The decline in recovery within the CEL can be interpreted as indicating damage to the microvasculature, which leads to leakage of contrast agent into the extravascular space. However, our results also showed an unexpected decrease in minimum recovery in the surrounding T2L for the grade III patient population (Tables 2 and 3). Minimum recovery refers to the lowest percent recovery value within a given region, indicating the greatest amount of BBB breakdown. Incomplete recovery in the non-enhancing region suggests that either the post-contrast T1-weighted imaging is not sensitive enough to detect all the damaged vessels or that the vessels are extremely tortuous. Patients with non-enhancing grade III gliomas showed a recovery pattern to that of the T2L-CEL region of the grade IV population (Table 4), further substantiating the differences observed above and the fact that the presence of enhancement may not always reflect the most malignant portion of the tumor.

Several published studies have looked at K^{trans} and other permeability measures in either low vs. high grade gliomas or individually in grade I, II, and III gliomas, excluding grade IV gliomas from their analysis (31, 42). In these studies, the authors either showed localized regions of increased permeability in high grade tumors compared to low grade tumors, or were unable to find any significant differences in K^{trans} between grades. The data presented in this manuscript is noteworthy in that our percent recovery parameter (which would be most closely associated with K^{trans}) was a sensitive enough measurement to detect significant differences between non-enhancing and enhancing tumor regions both within each patient cohort and between grade III and grade IV gliomas.

Abnormalities within the recirculation phase of the contrast agent bolus are often difficult to characterize and accurately interpret with respect to the underlying physiology. Kassner and Jackson et al. have previously described the implementation of a relative recirculation parameter (rR) as a way to characterize changes in the recirculation phase due to the presence of tortuous vessels that form in response to incomplete angiogenic processes (23, 29). According to this group, tortuosity manifests as both an increase in blood vessel volume, which is reflected by elevated rCBV (or in our case, aPH), and decreased signal recovery in the recirculation phase, as denoted by larger rR values (or reduced percent recovery). The additional presence of contrast enhancement would then suggest increased BBB breakdown in these tortuous vessels. If there is a concomitant increase in vessel volume, the reduction in recovery in non-enhancing tumor suggests the presence of tortuous but intact vessels. Similarly, the presence of contrast enhancement in patients with grade III gliomas is probably due to breakdown of the BBB, while grade IV gliomas are probably also experiencing a combination of angiogenesis and/or greater vascular tortuosity in the enhancing region.

While the clinical role of peak height and percent recovery as surrogate markers of abnormal vasculature requires further evaluation, the current study has shown that these parameters are useful in assessing tumor heterogeneity and the spatial variations of abnormal vasculature. The existence of contrast enhancement on T1-weighted post-gad images has been shown to underestimate tumor burden prior to therapy. Parametric maps of elevated peak height and abnormal recovery may be advantageous in treatment

planning, including target definition for conformal beam radiation therapy and biopsy guidance to help avoid underestimation of the histologic grading of non-enhancing tumors. Monitoring how both the magnitude and location of abnormality of these parameters change over time could prove advantageous in characterizing whether new contrast enhancement is due to radiation effects or tumor recurrence. Future assessment of the role of peak height and percent recovery as possible indicators of the effectiveness of novel anti-angiogenic therapies, as well as their ability to predict survival and regions of recurrence, would be of great interest. Although these parameters are currently limited in their ability to improve diagnostic accuracy in distinguishing grade III and grade IV gliomas, their potential in identifying more specific regions of vascular abnormality is still of great importance. The addition of other perfusion parameters and metabolic ratios may further elucidate the evolution of tumor progression, hopefully providing the necessary insight to achieve these goals.

Conclusions

Tumor microvasculature characteristics and their spatial distributions have shown considerable heterogeneity in grade III and grade IV glioma patients. Direct measurement of curve-shape parameters such as peak height and percent recovery has clearly improved specificity in characterizing these vascular changes in high grade gliomas compared to traditional rCBV calculations. Future studies will assess the prognostic value of these perfusion parameters in both predicting and evaluating tumor response to anti-angiogenic therapy for high grade glioma patients.

Acknowledgments

The authors thank Michael C. Lee, Pooja A. Sadarangani, Forrest C. Crawford, and Annette A. Chan of the Department of Radiology, UCSF for their assistance with data analysis or helpful comments regarding this manuscript.

References

1. Folkman J. **The role of angiogenesis in tumor growth.** *Semin Cancer Biol* 1992;3:65–71
2. Amoroso A, Del Porto F, Di Monaco C, Manfredini P, Afeltra A. **Vascular endothelial growth factor: a key mediator of neoangiogenesis: a review.** *Eur Rev Med Pharmacol Sci* 1997; 1:17–25
3. Brat DJ, Van Meir EG. **Glomeruloid microvascular proliferation orchestrated by VPF/VEGF: a new world of angiogenesis research.** *Am J Pathol* 2001;158:789–796
4. Wesseling P, Ruiter DJ, Burger PC. **Angiogenesis in brain tumors; pathobiological and clinical aspects.** *J Neurooncol* 1997;32:253–265
5. Damert A, Machein M, Breier G, et al. **Up-regulation of vascular endothelial growth factor expression in a rat glioma is conferred by two distinct hypoxia-driven mechanisms.** *Cancer Res* 1997;57: 3860–3864
6. Schneider SW, Ludwig T, Tatenhorst L, et al. **Glioblastoma cells release factors that disrupt blood-brain barrier features.** *Acta Neuropathol (Berl)* 2004;107:272–276
7. Pietsch T, Valter MM, Wolf HK, et al. **Expression and distribution of vascular endothelial growth factor protein in human brain tumors.** *Acta Neuropathol (Berl)* 1997;93:109–117
8. Jensen RL. **Growth factor-mediated angiogenesis in the malignant progression of glial tumors: a review.** *Surg Neurol* 1998;49:189–195
9. Lund EL, Spang-Thomsen M, Skovgaard-Poulsen H, Kristjansen PE. **Tumor angiogenesis: a new therapeutic target in gliomas.** *Acta Neurol Scand* 1998;97:52–62
10. Dachs GU, Chaplin DJ. **Microenvironmental control of gene expression: implications for tumor angiogenesis, progression, and metastasis.** *Semin Radiat Oncol* 1998;8:208–216
11. Stratmann A, Machein MR, Plate KH. **Anti-angiogenic gene therapy of malignant glioma.** *Acta Neurochir Suppl (Wien)* 1997;68: 105–110
12. Cha S, Knopp EA, Johnson G, et al. **Dynamic contrast-enhanced T2-weighted MR imaging of recurrent malignant gliomas treated with thalidomide and carboplatin.** *AJNR Am J Neuroradiol* 2000;21: 881–890
13. Chang L, McBride D, Miller BL, et al. **Localized in vivo 1H magnetic resonance spectroscopy and in vitro analyses of heterogeneous brain tumors.** *J Neuroimaging* 1995;5:157–163
14. Henry RG, Vigneron DB, Fischbein NJ, et al. **Comparison of relative cerebral blood volume and proton spectroscopy in patients with treated gliomas.** *AJNR Am J Neuroradiol* 2000;21:357–366
15. Assimakopoulou M, Sotiropoulou-Bonikou G, Maraziotis T, Papadakis N, Varakis I. **Microvessel density in brain tumors.** *Anticancer Res* 1997;17:4747–4753
16. Aronen HJ, Gazit IE, Louis DN, et al. **Cerebral blood volume maps of gliomas: comparison with tumor grade and histologic findings.** *Radiology* 1994;191:41–51
17. Griebel J, Mayr NA, de Vries A, et al. **Assessment of tumor microcirculation: a new role of dynamic contrast MR imaging.** *J Magn Reson Imaging* 1997;7:111–119
18. Cha S, Johnson G, Wadghiri YZ, et al. **Dynamic, contrast-enhanced perfusion MRI in mouse gliomas: correlation with histopathology.** *Magn Reson Med* 2003;49:848–855
19. Cha S, Knopp EA, Johnson G, Wetzel SG, Litt AW, Zagzag D. **Intracranial mass lesions: dynamic contrast-enhanced susceptibility-weighted echo-planar perfusion MR imaging.** *Radiology* 2002; 223:11–29
20. Guckel F, Brix G, Rempp K, Deimling M, Rother J, Georgi M. **Assessment of cerebral blood volume with dynamic susceptibility contrast enhanced gradient-echo imaging.** *J Comput Assist Tomogr* 1994;18:344–351
21. Knopp EA, Cha S, Johnson G, et al. **Glial neoplasms: dynamic contrast-enhanced T2*-weighted MR imaging.** *Radiology* 1999;211: 791–798
22. Chan A, Nelson S. **Simplified gamma variate fitting of perfusion curves.** From the Proceedings of the IEEE International Symposium of Biomedical Imaging, Arlington, VA, April 15–18, 2004: 1067–1070
23. Kassner A, Annesley DJ, Zhu XP, et al. **Abnormalities of the contrast re-circulation phase in cerebral tumors demonstrated using dynamic susceptibility contrast-enhanced imaging: a possible marker of vascular tortuosity.** *J Magn Reson Imaging* 2000;11:103–113
24. Weisskoff RM, Boxerman JL, Sorensen AG, Kulke SM, Campbell TA, Rosen BR. **Simultaneous blood volume and permeability mapping using a single Gd-based contrast injection.** From the Proceeding of the Society of Magnetic Resonance in Medicine, San Francisco, CA, August 6–12, 1994:279
25. Benner T, Heiland S, Erb G, Forsting M, Sartor K. **Accuracy of gamma-variate fits to concentration-time curves from dynamic susceptibility-contrast enhanced MRI: influence of time resolution, maximal signal drop and signal-to-noise.** *Magn Reson Imaging* 1997;15:307–317
26. Cha S, Lu S, Johnson G, Knopp EA. **Dynamic susceptibility contrast MR imaging: correlation of signal intensity changes with cerebral blood volume measurements.** *J Magn Reson Imaging* 2000;11:114–119
27. Jackson A, Kassner A, Zhu XP, Li KL. **Reproducibility of T2* blood volume and vascular tortuosity maps in cerebral gliomas.** *J Magn Reson Imaging* 2001;14:510–516
28. Chan A, Pirzkall A, Nelson S. **Analysis of serial changes in perfusion parameters for patients with recurrent high grade gliomas being treated with radiosurgery.** From the Proceedings of the International Society for Magnetic Resonance in Medicine, Kyoto, Japan, May 15–21, 2004
29. Jackson A, Kassner A, Annesley-Williams D, Reid H, Zhu XP, Li KL. **Abnormalities in the recirculation phase of contrast agent bolus passage in cerebral gliomas: comparison with relative blood volume and tumor grade.** *AJNR Am J Neuroradiol* 2002;23:7–14

30. Rosen BR, Belliveau JW, Vevea JM, Brady TJ. **Perfusion imaging with NMR contrast agents.** *Magn Reson Med* 1990;14:249–265
31. Provenzale JM, Wang GR, Brenner T, Petrella JR, Sorensen AG. **Comparison of permeability in high-grade and low-grade brain tumors using dynamic susceptibility contrast MR imaging.** *AJR Am J Roentgenol* 2002;178:711–716
32. Li KL, Zhu XP, Checkley DR, et al. **Simultaneous mapping of blood volume and endothelial permeability surface area product in gliomas using iterative analysis of first-pass dynamic contrast enhanced MRI data.** *Br J Radiol* 2003;76:39–50
33. Tofts PS, Brix G, Buckley DL, et al. **Estimating kinetic parameters from dynamic contrast-enhanced T(1)-weighted MRI of a diffusable tracer: standardized quantities and symbols.** *J Magn Reson Imaging* 1999;10:223–232
34. Tofts PS. **Modeling tracer kinetics in dynamic Gd-DTPA MR imaging.** *J Magn Reson Imaging* 1997;7:91–101
35. Roberts HC, Roberts TP, Brasch RC, Dillon WP. **Quantitative measurement of microvascular permeability in human brain tumors achieved using dynamic contrast-enhanced MR imaging: correlation with histologic grade.** *AJNR Am J Neuroradiol* 2000;21:891–899
36. Jackson A, Jayson GC, Li KL, et al. **Reproducibility of quantitative dynamic contrast-enhanced MRI in newly presenting glioma.** *Br J Radiol* 2003;76:153–162
37. Miyati T, Banno T, Mase M, et al. **Dual dynamic contrast-enhanced MR imaging.** *J Magn Reson Imaging* 1997;7:230–235
38. Barbier EL, den Boer JA, Peters AR, Rozeboom AR, Sau J, Bonmartin A. **A model of the dual effect of gadopentetate dimeglumine on dynamic brain MR images.** *J Magn Reson Imaging* 1999;10:242–253
39. Vonken EP, van Osch MJ, Bakker CJ, Viergever MA. **Simultaneous quantitative cerebral perfusion and Gd-DTPA extravasation measurement with dual-echo dynamic susceptibility contrast MRI.** *Magn Reson Med* 2000;43:820–827
40. Heiland S, Benner T, Debus J, Rempp K, Reith W, Sartor K. **Simultaneous assessment of cerebral hemodynamics and contrast agent uptake in lesions with disrupted blood-brain-barrier.** *Magn Reson Imaging* 1999;17:21–27
41. Law M, Yang S, Wang H, et al. **Glioma grading: sensitivity, specificity, and predictive values of perfusion MR imaging and proton MR spectroscopic imaging compared with conventional MR imaging.** *AJNR Am J Neuroradiol* 2003;24:1989–1998
42. Law M, Yang S, Babb JS, et al. **Comparison of cerebral blood volume and vascular permeability from dynamic susceptibility contrast-enhanced perfusion MR imaging with glioma grade.** *AJNR Am J Neuroradiol* 2004;25:746–755
43. Rueckert D, Sonoda LI, Hayes C, Hill DL, Leach MO, Hawkes DJ. **Nonrigid registration using free-form deformations: application to breast MR images.** *IEEE Trans Med Imaging* 1999;18:712–721
44. Studholme C, Hill D, Hawkes D. **An overlap invariant entropy measure of 3D medical image alignment.** *Pattern Recognition* 1999;32:71–86
45. Crawford F, Cha S, Lupo JM, et al. **Predicting the emergence of contrast enhancement in glioblastoma multiforme using bolus tracking perfusion MRI.** From the Proceedings of the International Society for Magnetic Resonance in Medicine, Kyoto, Japan, May 15–21, 2004
46. Andersen C, Jensen FT. **Differences in blood-tumour-barrier leakage of human intracranial tumours: quantitative monitoring of vasogenic oedema and its response to glucocorticoid treatment.** *Acta Neurochir (Wien)* 1998;140:919–924
47. Law M, Cha S, Knopp EA, Johnson G, Arnett J, Litt AW. **High-grade gliomas and solitary metastases: differentiation by using perfusion and proton spectroscopic MR imaging.** *Radiology* 2002;222:715–721
48. Fan G, Sun B, Wu Z, Guo Q, Guo Y. **In vivo single-voxel proton MR spectroscopy in the differentiation of high-grade gliomas and solitary metastases.** *Clin Radiol* 2004;59:77–85